Introduction to paper, "Study of Conversion and Partitioning of Wave Energies at Different Kinds of Boundaries in Fluid-Saturated Porous Media" by K.C. Balan and M.H. Engineer

Conventional theory of wave propagation assumes that the medium through which the wave is propagating consists of a single phase. One tries to account for the effect of heterogeneity and fluid inclusions in the medium indirectly by replacing the multi-phase medium by a single phase medium with effective elastic parameters. This model is valid only to the extent that the relative motion of the fluid with respect to the solid phase can be ignored. In 1956, M A Biot published a seminal paper, " Theory of propagation of elastic waves in a fluid saturated porous solid, I – low frequency range" in Journal of Acoustic Society of America, which rigorously described wave propagation in a two-phase medium. The theory predicts, in addition to the S-wave, two types of dilatational waves, D1 & D2, where D1 is a higher velocity wave akin to the conventional wave in an effective single phase medium and D2 is a lower velocity diffusive wave describing the fluid motion relative to the surrounding solid matrix. An important parameter in Biot's theory is a characteristic frequency $\omega_c = \nu\Phi / (\kappa_0\alpha)$, where ν is the kinematical viscosity, Φ is the porosity, κ_0 is the zero frequency permeability, and α is the tortuousity of the medium. Below this critical frequency, the viscous effects dominate and the two phases effectively move together as one. However, as frequency becomes of the order of ω_c, or higher, D2 wave carries a significant fraction of the total energy in wave propagation. Predictions of Biot's theory have been extensively verified in laboratory studies.

An important, but not yet adequately studied, consequence of Biot's theory is regarding the predictions for Amplitude vs. Angle (AVA). When a dilatational wave (D1) is incident at an interface of two 2-phase media, we obtain three types of waves (D1, D2, S) in each of the two media. Consequently, application of the boundary conditions, namely, continuity of displacements and stresses for these three types of waves across the interface, leads to a 6 X 6 matrix equation for the reflection and transmission coefficients of these three waves. This is in contrast to a 4 X 4 matrix equation derived by Zoeppritz for the reflection & transmission coefficients (for one dilatational and one shear wave) which forms the basis of all qualitative & quantitative AVA analysis, currently.

In 1979, Balan & Engineer, working at ONGC, derived this 6 X 6 matrix equation in the frame-work of Biot's theory and analyzed the AVA at an interface of two fluid-saturated media for different parameters, particularly porosities, of the media. The difference in the predictions for AVA, based on 4 X 4 Zoeppritz equation and 6 X 6 equation used by Balan and Engineer, would be significant for high end of the seismic frequency spectrum – especially for gas saturated sediments. Extension of this work to rocks with partially saturated viscous fluids will prove useful for quantitative analysis of saturants. We reproduce here this internal report with scanned images with minor editing.

…… **Editor**

Study of Conversion and Partitioning of Wave Energies at Different Kinds of Boundaries in Fluid-Saturated Porous Media

K C Balan & M H Engineer, ONGC, Dehradun*

Recently, it has been shown that seismic reflection exploration can also indicate the actual presence of hydrocarbon accumulations in the structures (Pan et. al. (1)). To date, these so called 'Bright spot' – techniques have been somewhat successful in locating gas zones only. To sustain and improve this success one must go beyond the correct, but limited notion of the 'Bright Spot' technique, that the relatively low acoustic impedance of trapped gas gives rise to large reflection amplitudes and, hence, all that is required is to look for the amplitude anomalies giving rise to bright, dim or flat spots on the sections.

Some work has already been done in this direction. The basic idea underlying in this work is that potential hydrocarbon reservoirs will show some distinctive features which stand out against the background. Much effort is also being made to better extract the information regarding the seismic traces while keeping the basic bright spot notions (Anstey (2)). The effect of water saturation on the reflectively at a reservoir interface has been studied by Domenico (3). His work suggests that water cannot be detected from reflection amplitudes in gas sands, but may, under optimum conditions be detected in oil sands. Crowe and Alhilali (4) have gone a step ahead and studied the attenuation problem for the various types of loss mechanisms postulated in the literature and relevant to the case at hand.

In these above-mentioned works a rigorous theory for the basic formulation of the problem of seismic wave propagation in fluid filled porous rocks is lacking. Nevertheless, the literature does contain a work that overcomes the defect to some extent. The pioneering works of Biot (5, 6) are the most important ones, since he alone takes into account the coupling of fluid and solid motions induced by a traveling sound wave. All other approaches (we discuss the important ones in section 2) average this coupling out of the physics. The relative motion between the fluid and the solid, for a viscous fluid, leads to a characteristic attenuation of the sound wave energy. Using Biot's work, we can calculate this important effect which will then provide us with a possible basis for discriminating between water and hydrocarbons in the reservoir rocks.

However, in order to apply the results of Biot's formulation to practical cases in oil exploration, we must study the problems of conversion and partitioning of wave energy when the waves undergo reflection and transmission at an interface of two fluid saturated porous media (hereafter referred to as composite medium). Using Biot's theory, Geertsma and Smit (7) have studied the partitioning of energy at the interface between two composite media for a normally incident wave only. Our program is to make a detailed investigation of the energy partitioning as a function of angle, porosity and saturants in various situations of exploration interest.

We discuss here the case of a monochromatic incident wave when the saturant is an inviscid fluid. We present the variation of the reflection and transmission coefficients and various wave energies as a function of the angle of incidence, the porosity and the saturant.

In section 2 we briefly discuss the earlier works dealing with sound propagation in composite media and indicate each one's usefulness, in the bright spot field. In section 3 we outline and discuss Biot's theory (5). In section 4 we study the conversion and partitioning of energy when the incident wave encounters a rigid boundary of a composite medium. This is relevant to the reflection at the hard bottom of a porous reservoir. In section 5 we do the above analysis for the case of a stress-free boundary of a composite medium. This is relevant at the top surface of the weathering layer. Section 6 deals with the case of an interface of two composite media. In all these sections we have calculated the partitioning of amplitudes and energies, and have discussed the variation of these with the angle of incidence and the porosity. For a quick study of the variation with the angle of incidence and porosity, the plots of energies and the reflection and transmission coefficients are presented for different values of the porosity parameter. In section 7 we list out the major conclusions made in this study.

2. Discussion of previous works:

The field of wave propagation through composite media is comparatively new. In 1951, Gassman (8) has taken the initiative and has tried to model a porous medium and study the wave propagations through it. He has emphasized the role of elasticity of the solid skeleton in the problem. Later, Ament (9) and Wyllie et. al. (10, 11) have continued to work on these lines. The theoretical and experimental work of Wyllie leading to the much used time-average equation relating seismic velocity to porosity has been a major breakthrough in the subject. His time-average equation has been shown to be useful in different cases like (i) sandstones subjected to high differential pressures, (ii) completely liquid mixtures (iii) completely cemented sandstones and (iv) sometimes, for unfractured limestones (here the evidence is not very clear). The time-average equation is not true for shales. The work of Domenico (3) gives an up to date

* This work was done by the authors in 1978 at KDMIPE, ONGC, Dehradun

discussion of the effect of fluid saturation on the wave propagation in a porous medium. He concludes that the highly non-linear velocity porosity relation given by Woods (12) has some experimental justification in air-earth mixtures.

A very rigorous mathematical theory has been supplied by Biot (5) for the wave propagation through porous media when the saturant is either inviscid or viscous. Since then, his theory has been used by some workers in the field. Later, Biot (13, 14) further investigated acoustic wave propagation and the dissipative mechanism in a porous medium.

The theoretical and experimental investigations carried out by Toksoz et al (15) and Kustor and Toksoz (15, 16) using the method of scattering is another major advance in the field. The theory is valid for (1) a solid medium with solid and liquid inclusions and (2) a solid suspension in a fluid matrix, when the concentration of inclusions is small. The authors have discussed the effects of inclusion concentrations and shapes on the effective elastic modulii and velocities. In all the cases, the effective elastic modulii and velocities decrease with increasing concentration of inclusions. For a given concentration the flatter inclusions have greater effect than the rounder ones. Even a very low concentration (0.01 percent) of thin inclusions could decrease the velocities in the composite medium by as much as 10 percent. The authors also discuss the effects of water or gas saturation on the wave velocities. They conclude that these depend very much on the pore shapes. For example, when the pores are of spherical shape, the velocity increases as the water saturation decreases, whereas for intermediate pore shapes (such as these with aspect ratio – the ratio of minimum to maximum diameter – of about 0.1) the variation in velocity with water saturation is insignificant. For thin pores and cracks both P and S velocities decrease with the water saturation. It has to be noted that variation in P wave velocity is far more dominant. The experimental part of the work measures the velocity and attenuation of waves in suspensions of solid spherical particles in fluid matrices as a function of the concentration of inclusions at ultrasonic frequencies. Close agreement with the theoretical investigation was obtained.

Biot's theory has been used by Stoll (17, 18) and Stoll et. al. (19), to predict the effects of porosity, grain size and permeability on the energy loss of seismic waves in the unconsolidated ocean sediments. They have discussed the energy loss arising from two kinds of mechanisms: (i) relative fluid flow in the pores as in Biot (5) and (ii) the inter-granular losses in the skeletal frame. The frequency dependent attenuation and velocity of shear and dilatational waves have been studied and plotted against the frequency, at different depths below the sea floor. The variation of reflection coefficients with frequency for normal incidence of dilatational waves, in water over sand, is also studied.

Quite a few workers have tried to develop a constitutive theory for the effective stress-strain fields in a composite medium. The recent contributions are due to Garg (20), Garg and Nur (21), Nur and Byerlee (22), and Moreland (23).

3. Theory :

The theory developed by Biot (5) for the propagation of seismic waves through a composite medium, has been made use of. If the volume fraction of the fluid completely filling the pores is Ö then the effective density of the medium is :

$$\rho = \rho_s(1-\phi) + \rho_f\phi \qquad (3.1)$$

where ρ_s is the density of the solid, which forms the matrix,and is the density of the fluid, which forms the inclusions. The basic equations governing the propagation of dilatational waves through a porous media are (with in Biot's theory) :

$$\nabla^2(Pe+QE) = \frac{\partial^2}{\partial t^2}(\rho_1 e) \qquad (3.2)$$

$$\nabla^2(Qe+RE) = \frac{\partial^2}{\partial t^2}(\rho_2 E) \qquad (3.3)$$

where ^{2} is the usual Laplacian operator and e and E are the dilatation in the solid and the fluid respectively. P and R are the elastic constants (P= A_s + 2N_s, R = A_f where A and N are the usual Lame's Coefficients of the medium; suffixes s and f indicate solid and fluid respectively) of the matrix and the inclusions; Q is the coupling parameter and

$$\rho_1 = \rho_s(1-\phi) \qquad (3.4)$$

$$\rho_2 = \rho_f\phi \qquad (3.5)$$

The constants, P, Q and R, which describe the elastic response of the composite medium, have themselves been a subject of considerable interest (21, 22, 23). These constants are to be determined by static elastic experiments.

In the following, the constant N appearing is N_s; the suffix s is dropped for convenience.

The equation governing the propagation of the rotational waves are:

$$N\nabla^2\omega = \frac{\partial^2}{\partial t^2}(\rho_1\omega) \qquad (3.6)$$

$$0 = \frac{\partial^2}{\partial t^2}(\rho_2\Omega) \qquad (3.7)$$

where ù and Ù are the rotations in the solid and the

fluid - given by the curl of the displacement vector fields. The typical values taken for , P, Q, and R in the following numerical calculations and the computer plots are:

= 2.7 gms/cc
= 0.8 gms/cc
A_s = 0.6 x 10^{11} dynes/cm^2
N_s = 0.5 x 10^{11} dynes/cm^2
Q = 0.1 x 10^{11} dynes/cm^2
R = 1.25 x 10^{11} dynes/cm^2

With these typical values, the velocities of the different waves for different porosity are tabulated in Table I, II & III

TABLE – I

$\rho_s = 2.6 gm/cc$, $\rho_f = 0.9 gm/cc$, A=0.8E, N=0.6E, Q=0.1E, R= 0.25 E, where E = 10^{11} dynes/ cm^2

Porosity Ö (fraction)	ρ_1	ρ_2	V_{D1} (km/sec)	V_{D2} (km/sec)	V_s (km/sec)
0.05	2.47	0.045	7.45	2.81	1.56
0.1	2.34	0.09	5.29	2.88	1.6
0.15	2.21	0.135	4.34	2.95	1.65
0.2	2.08	0.18	3.8	3.01	1.7
0.25	1.95	0.225	3.5	3.02	1.75

TABLE – II

$\rho_s = 2.6 gm/cc$, $\rho_f = 0.7 gm/cc$, A=0.65 E, N=0.55E, Q=0.05E, R=0.2E, where E = 10^{11} dynes/ cm^2

Porosity Ö (fraction)	ρ_1	ρ_2	V_{D1} (km/sec)	V_{D2} (km/sec)	V_s (km/sec)
0.1	2.34	0.07	5.35	2.72	1.53
0.2	2.08	0.14	3.8	2.86	1.63
0.3	1.82	0.21	3.22	2.96	1.74

TABLE – III

$\rho_s = 2.7 gm/cc$, $\rho_f = 0.8 gm/cc$, A=0.6E, N=0.5E, Q=0.1E, R=0.25E where E = 10^{11} dynes/ cm^2

Porosity Ö (fraction)	ρ_1	ρ_2	V_{D1} (km/sec)	V_{D2} (km/sec)	V_s (km/sec)
0.05	2.565	0.04	7.92	2.46	1.40
0.1	2.43	0.08	5.61	2.53	1.44
0.2	2.16	0.16	4.0	2.66	1.52

We use following notations:
u = the displacement vector in the solid
U = the displacement vector in the fluid in the pores
The basic equations are solved for three types of geometries:

a) Rigid boundary of a composite medium
b) Stress free boundary of a composite medium
c) Interface of two composite media

An incident wave encountering any one of these boundaries can be either a dilatational wave of 1st or 2nd kind hereafter referred to as D1 and D2 wave or a shear wave (see appendix 1). The set of boundary conditions for the above three boundaries are:

(a) All solid displacement components and the normal component of fluid displacement should vanish at rigid boundary;
(b) All solid stress components and normal fluid stress must vanish at a stress free boundary
(c) The above said solid and fluid stress-displacement components should be continuous across an interface of two composite media.

Now we discuss each boundary separately.

4. Rigid boundary of a composite media:

In all the following discussions we convert the basic equations (3.2), (3.3), (3.6) and (3.7) into equations for the displacement potentials ϕ_s, ϕ_l and Ψ_s where the displacement vector in (x, z) plane is decomposed as:

$$u = \nabla\phi_s + \nabla \times \Psi_s \qquad (4.1)$$

$$U = \nabla\phi_l \qquad (4.2)$$

with usual notations for the gradient and curl operator. The vector field is chosen as (0, $_s$, 0).

(gm/cc)

For the case of a D1 – incident wave (dilatational wave of first kind), the potentials and are written in the form (in all the following expressions the time dependence exp [iwt] is removed throughout for the sake of convenience).

$$\phi_s = \phi_{si}\exp[i(az - bx)] + \phi_{sr1}\exp[-i(az + bx)] + \phi_{sr2}\exp[-i(a_1 z + b_1 x)] \quad (4.3)$$

$$\phi_l = \phi_{li}\exp[i(az - bx)] + \phi_{lr1}\exp[-i(az + bx)] + \phi_{lr2}\exp[-i(a_1 z + b_1 x)] \quad (4.4)$$

and is given by:

$$\psi_s = \psi_{sr}\exp[-i(a_2 z + b_2 x)] \qquad (4.5)$$

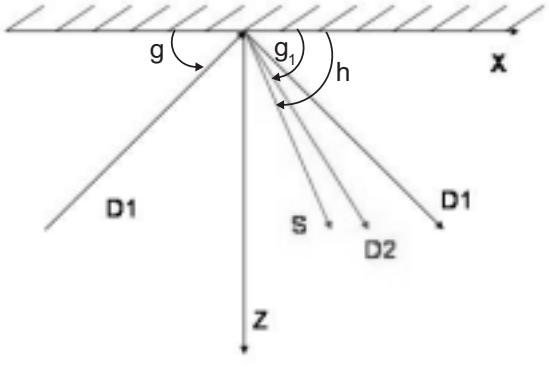

Fig.4.1 Diagram showing wave D1 incident on a rigid insect boundary in a porous medium with D1, D2 and S reflected waves.

The suffix 's' stands for solid, '*l*' for liquid, 'i' for incident wave and 'r' for reflected wave. The above expressions represent a D1 incident wave, D1–reflected wave, D2-reflected wave and shear reflected wave. The boundary conditions at the rigid boundary (z=0) would demand that apparent velocity of all waves along the x-axis is same i.e. b=b1=b2. Applying the boundary conditions (appendix 2), we get the reflection coefficients in the form:

$$A\,R = B \qquad (4.6)$$

where A is a 3 x 3 matrix:

$$A = \begin{bmatrix} 1 & 1 & -T_2 \\ T & T_1 & 1 \\ \beta_1 T & \beta_2 T_1 & 0 \end{bmatrix} \qquad (4.7)$$

B is a column vector given by:

$$B = \begin{bmatrix} -1 \\ T \\ \beta_1 T \end{bmatrix} \qquad (4.8)$$

and R is the column vector of the reflection coefficients given by,

$$R = \begin{bmatrix} r_1 \\ r_2 \\ r_s \end{bmatrix} \qquad (4.9)$$

where r_1, r_2 and r_s are the reflection coefficients of D1-wave, D2 wave and shear wave respectively. T, T_1 and T_2 are the tangents of the angle of incidence of D1 wave (g), the angle of emergence of D2 wave (g1) and the angle of emergence of shear wave (h) respectively (all measured from the plane of the rigid boundary).

$$T = \tan g = a/b \qquad (4.10a)$$

$$T_1 = \tan g_1 = a_1/b \qquad (4.10\,b)$$

$$T_2 = \tan h = a_2/b \qquad (4.10\,c)$$

$$r_1 = \phi_{sr1}/\phi_{si} \qquad (4.11a)$$

$$r_2 = \phi_{sr2}/\phi_{si} \qquad (4.11b)$$

$$r_s = \psi_{sr}/\phi_{si} \qquad (4.11c)$$

and are the parameters coupling the solid and the fluid potentials by the relations:

$$\phi_{li} = \beta_1 \phi_{si} \qquad (4.12a)$$

$$\phi_{lr1} = \beta_1 \phi_{sr1} \qquad (4.12b)$$

$$\phi_{lr2} = \beta_2 \phi_{sr2} \qquad (4.12c)$$

and these are obtained from the basic equations (3.2) and (3.3) as

$$\beta_1 = -\left(\frac{P - \rho_1\alpha_1^2}{Q}\right) = -\left(\frac{Q}{R - \rho_2\alpha_1^2}\right) \qquad (4.13\,a)$$

$$\beta_2 = -\left(\frac{P - \rho_1\alpha_2^2}{Q}\right) = -\left(\frac{Q}{R - \rho_2\alpha_2^2}\right) \qquad (4.13\,b)$$

and are the velocities of D1 and D2 waves, respectively.

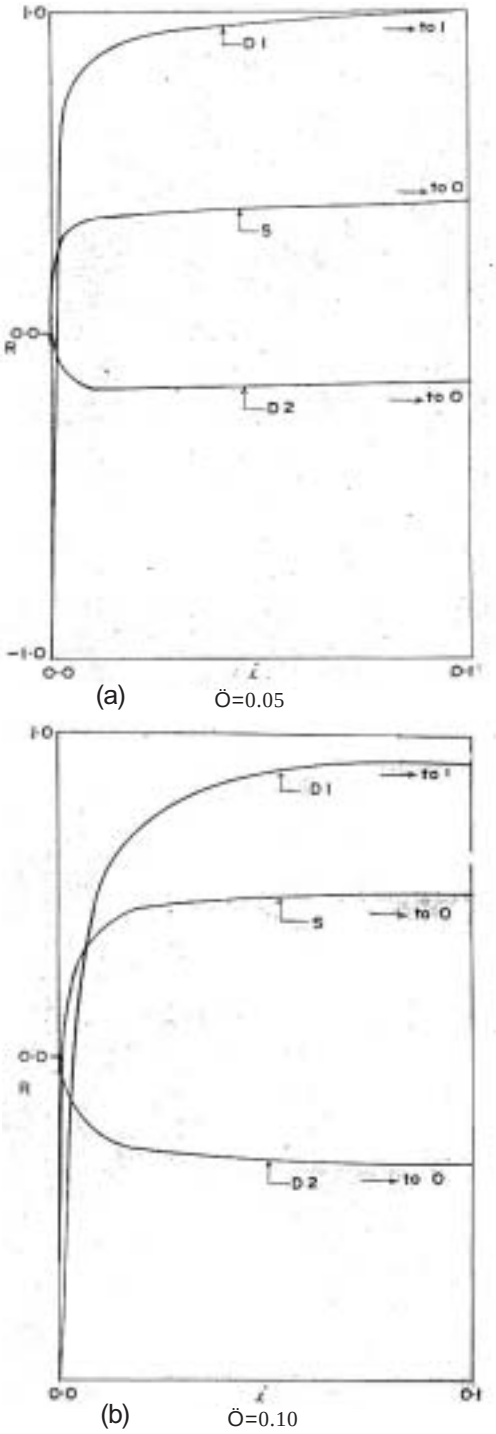

Fig.4.2 Reflectivity at rigid boundary as a function of incident angle *i* in radians for incident D1-wave for (a) porosity Ö=0.05 (b) Ö=0.10

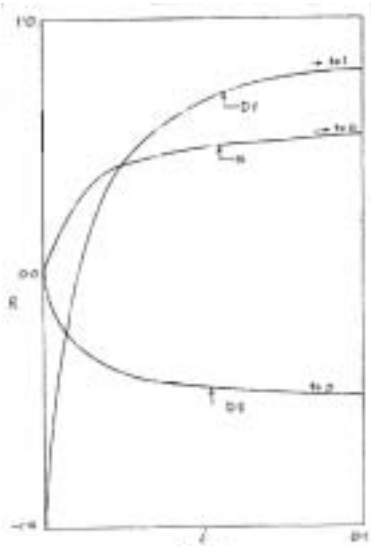

Ö=0.15

Fig.4.3 Reflectivity at rigid boundary as a function of incident angle *i* in radians for incident D1-wave for porosity Ö=0.15

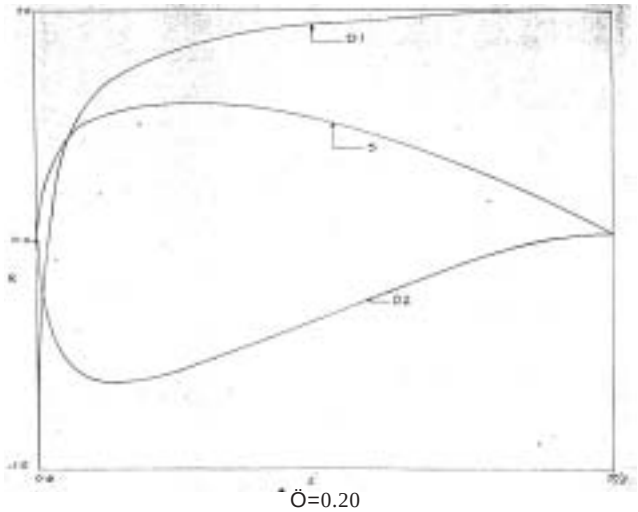

Ö=0.20

Fig.4.4 Reflectivity at rigid boundary as a function of incident angle *i* in radians (0, ð/2) for incident D1-wave for porosity Ö=0.2

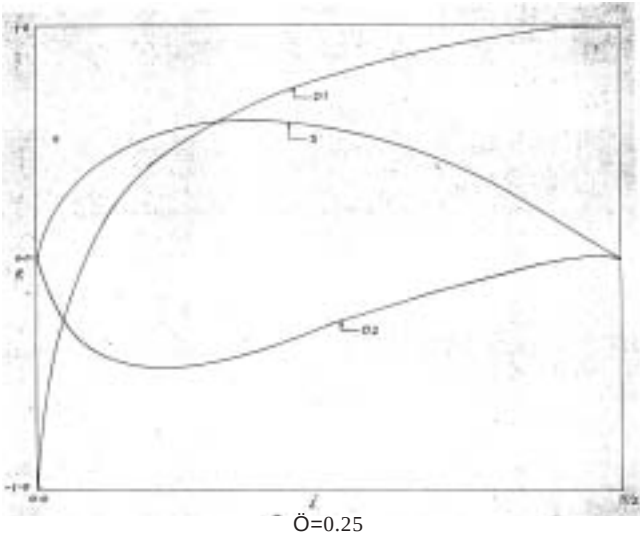

Ö=0.25

Fig.4.5 Reflectivity at rigid boundary as a function of incident angle *i* in radians (0, ð/2) for incident D1-wave for porosity Ö=0.25

The procedure of obtaining and is given in appendix (1). The set of equations (4.6) is solved for the vector R and the reflection coefficients are obtained as functions of the angle of incidence and the porosity . For a better understanding they are plotted against the angle of incidence in figures (4.2) to (4.5) for porosity parameter ϕ ranging from 0.05 to 0.25. For grazing (g=0) and normal incidence, D2 and shear wave amplitudes vanish, as is expected. As g varies from grazing to normal incidence, r_1 increases from -1 to +1. The coefficients r_2 and r_s first vary rapidly from zero to an extreme (say r_{2m} and r_{sm}) which are attained at an angle close to zero (say i_{ex}) and then steadily go to zero as i . The variation in r_1 is predominant essentially in the interval $(0, i_{ex})$. As increases, the range $(0, i_{ex})$ becomes wider and r_{2m} and r_{sm} grow in magnitude. For large ϕ , the tendency is to make the variation with g smoother. The primary conclusion is that the effect of ϕ on r_1, r_2 and r_s for near normal incidence is insignificant. For moderate angle of incidence the effect of increasing ϕ is to increase the conversion of waves.

Energy considerations :

With the knowledge of the wave velocities and the potentials one can now compute the energy carried by each of the waves. The incident wave energy is

$$\frac{1}{2}\rho_1\varphi_{si}^{\ 2}\omega^2 b^2\alpha_1\sec^2 g\sin g + \frac{1}{2}\rho_2\varphi_{li}^{\ 2}\omega^2 b^2\alpha_1\sec^2 g\sin g \qquad (4.14)$$

The reflected D1 wave energy is

$$\frac{1}{2}\rho_1\varphi_{sr1}^2\omega^2 b^2\alpha_1\sec^2 g\sin g + \frac{1}{2}\rho_2\varphi_{lr1}^2\omega^2 b^2\alpha_1\sec^2 g\sin g \qquad (4.15)$$

The reflected D2 – wave energy is

$$\frac{1}{2}\rho_1\varphi_{sr2}^2\omega^2 b^2\alpha_2\sec^2 g_1\sin g_1 + \frac{1}{2}\rho_2\varphi_{lr2}^2\omega^2 b^2\alpha_2\sec^2 g_1\sin g_1 \qquad (4.16)$$

The reflected shear wave energy is

$$\frac{1}{2}\rho_1\psi_{sr}^2\omega^2 b^2\alpha_3\sec^2 h\sin h \qquad (4.17)$$

where is the shear wave velocity. The law of conservation of energy reduces to the equation:

$$r_1^2 + \left(\frac{\rho_1+\rho_2\beta_2^2}{\rho_1+\rho_2\beta_1^2}\right)\frac{T_1}{T}r_2^2 + \left(\frac{\rho_1}{\rho_1+\rho_2\beta_1^2}\right)\frac{T_2}{T}r_s^2 = 1 \qquad (4.18)$$

The square root of these wave energy ratios are plotted against the angle of incidence in figures (4.6) to (4.9). Here also there is a critical value of the angle of incidence at which the energy carried by the waves reaches an extremum as shown in the plots.

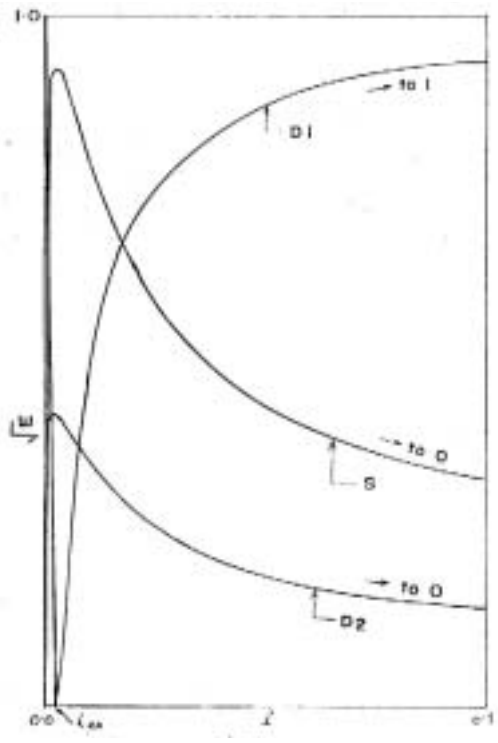

(a) Ö=0.10

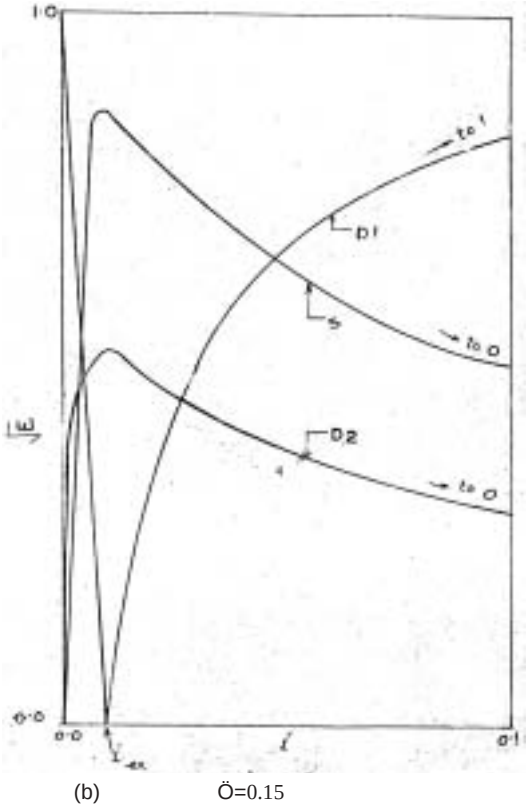

(b) Ö=0.15

Fig.4.6 Square root of Energy ratio at rigid boundary as a function of incident angle *i* in radians for incident D1-wave for (a) porosity Ö=0.1 **,** (b) Ö=0.15. Angle i_{ex} is the one for which D1 is minimum

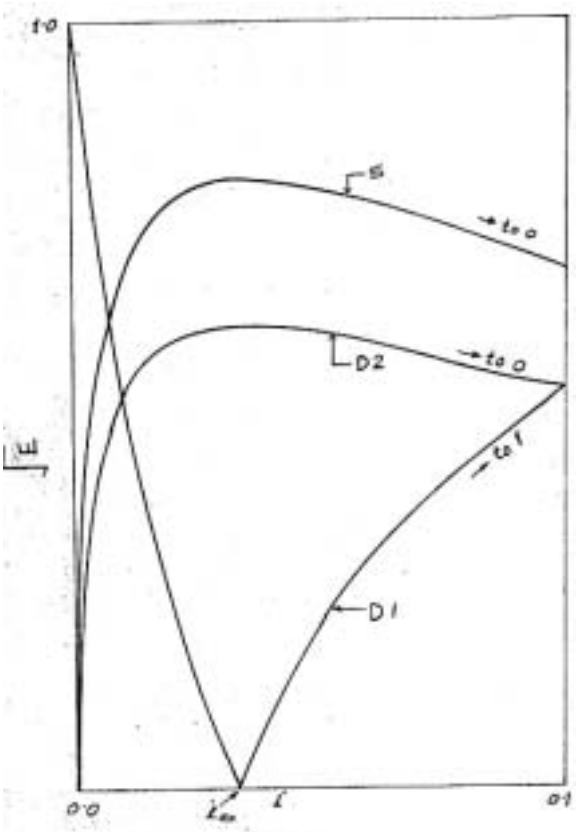

Ö=0.20

Fig.4.7 Square root of Energy ratio at rigid boundary as a function of incident angle *i* in radians for incident D1-wave for porosity Ö=0.2 . Angle $\mathbf{i}_{ex}$ is the one for which energy of D1 is minimum

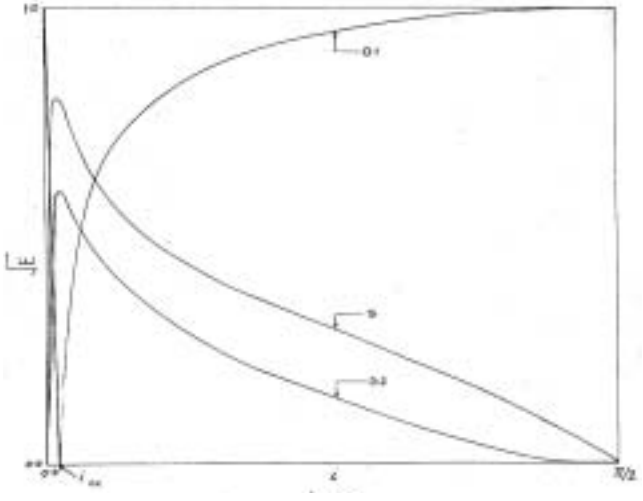

Ö=0.20

Fig.4.8 Same as for Fig 4.7 except that the angle of incidence is up to ð/2

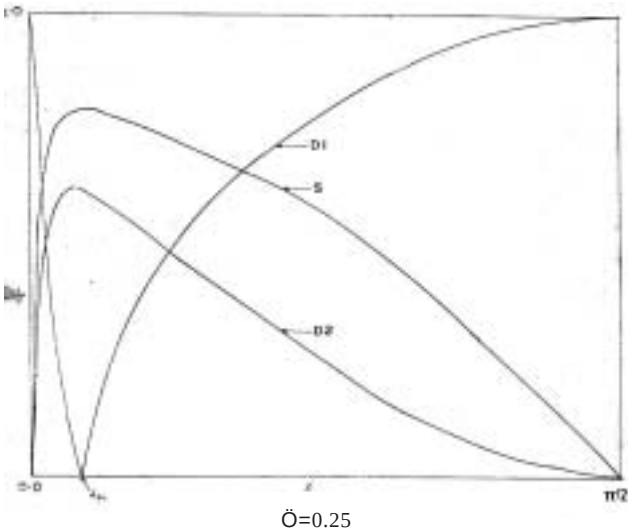

Ö=0.25

Fig.4.9 Square root of Energy ratio at rigid boundary as a function of incident angle *i* in radians (0, ð/2) for incident D1-wave for porosity Ö=0.25 . Angle $\mathbf{i}_{ex}$ is the one for which energy of D1 is minimum

For the case of a D2 wave incident, the expressions for , and are

$$\phi_s = \phi_{si}\exp[i(a_1 z - bx)] + \phi_{sr1}\exp[-i(az + bx)] + \phi_{sr2}\exp[-i(a_1 z + bx)] \quad (4.19)$$

$$\phi_l = \phi_{li}\exp[i(a_1 z - bx)] + \phi_{lr1}\exp[-i(az + bx)] + \phi_{lr2}\exp[-i(a_1 z + bx)] \quad (4.20)$$

$$\psi_s = \psi_{sr}\exp[-i(a_2 z + bx)] \quad (4.21)$$

The energy conservation law in this case is

$$\left(\frac{\rho_1 + \rho_2\beta_1^2}{\rho_1 + \rho_2\beta_2^2}\right)\frac{T}{T_1}r_1^2 + r_2^2 + \left(\frac{\rho_1}{\rho_1 + \rho_2\beta_2^2}\right)\frac{T_2}{T_1}r_s^2 = 1 \quad (4.23)$$

As the velocity of the D2 wave is less than that of D1 wave, there exists a certain angle of incidence below which the D1 reflected waves are not generated at the boundary and hence, in the plots presented here, the whole range (0,) of angle in incidence is not covered. This critical value of the angle of incidence is close to, but less than the lower limit in the respective plots. As increases this critical angle of incidence moves towards the zero value. For small porosity ϕ, ~0; as ϕ increases, and r_2 grow in magnitude and more conversion of energy takes place into D1 and shear waves until a certain porosity (which lies between 0.2 and 0.25) beyond which the shear wave energy decreases. We conclude that as $\phi \to 1$ (in which case the medium will behave like a fluid), the shear wave energy will disappear.

Fig. 4.10 to Fig 4.15 depict the reflectivities for D2 wave incident on a rigid boundary for different medium porosities.

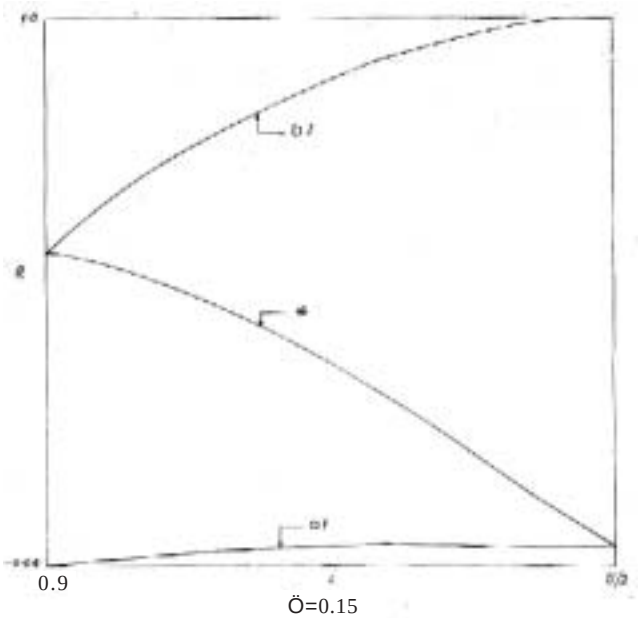

Ö=0.15

Fig.4.10 Reflectivity at rigid boundary as a function of incident angle *i* in radians (0.9, ð/2) for incident D2-wave for porosity Ö=0.15

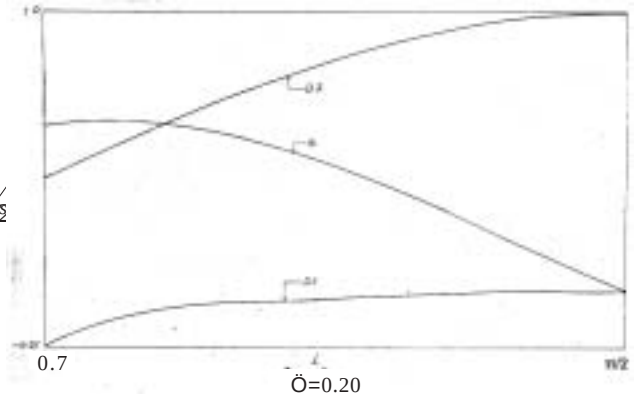

Ö=0.20

Fig.4.11 Reflectivity at rigid boundary as a function of incident angle *i* in radians (0.7, ð/2) for incident D2-wave for porosity Ö=0.20

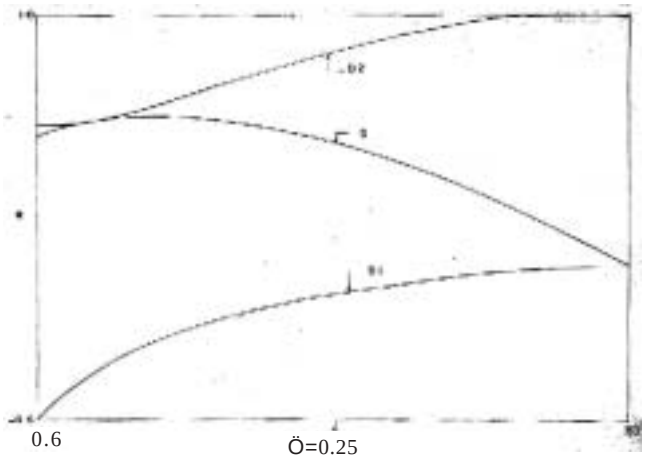

Ö=0.25

Fig.4.12 Reflectivity at rigid boundary as a function of incident angle *i* in radians (0.6, ð/2) for incident D2-wave for porosity Ö=0.25

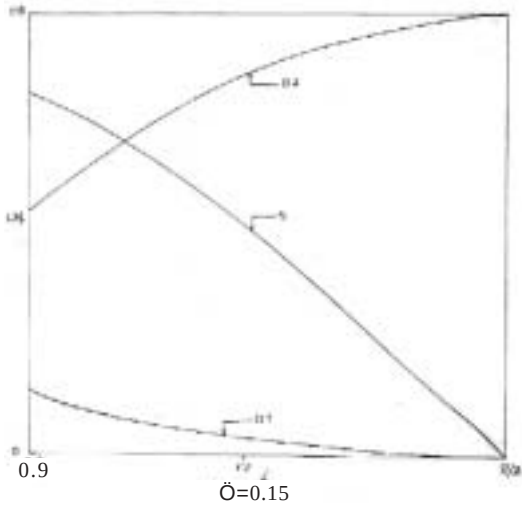

Fig.4.13 Square root of Energy ratio at rigid boundary as a function of incident angle *i* in radians (0.9, ð/2) for incident D2-wave for porosity Ö=0.15

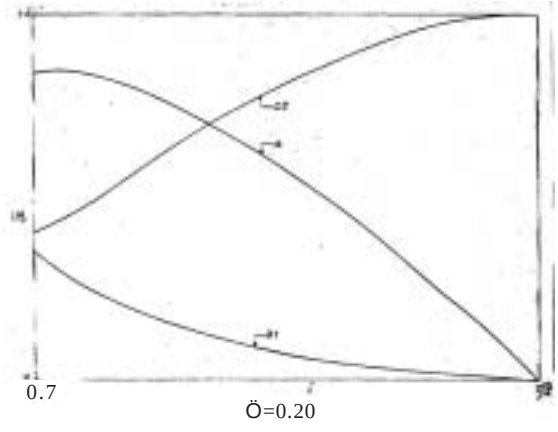

Fig.4.14 Square root of Energy ratio at rigid boundary as a function of incident angle *i* in radians (0.7, ð/2) for incident D2-wave for porosity Ö=0.2

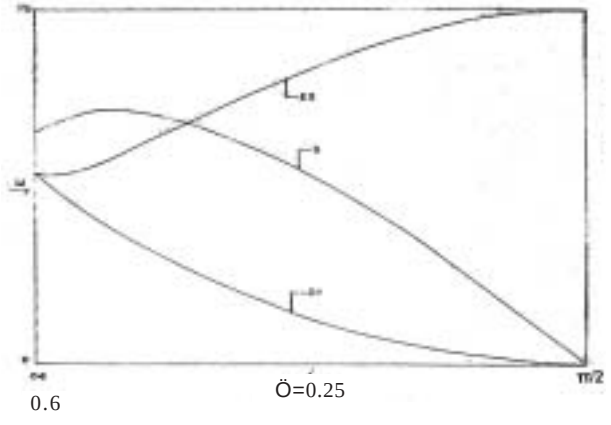

Fig.4.15 Square root of Energy ratio at rigid boundary as a function of incident angle *i* in radians (0.6, ð/2) for incident D2-wave for porosity Ö=0.25

When a shear wave is incident, the expressions for ϕ_s, ϕ_l and ψ_s are

$$\phi_s = \phi_{sr1}\exp[-i(az+bx)]+\phi_{sr2}\exp[-i(a_1z+bx)] \quad (4.24)$$

$$\phi_l = \phi_{lr1}\exp[-i(az+bx)]+\phi_{lr2}\exp[-i(a_1z+bx)] \quad (4.25)$$

$$\psi_s = \psi_{si}\exp[i(a_2z-bx)]+\psi_{sr}\exp[-i(a_2z+bx)] \quad (4.26)$$

Again, the matrix A remains the same (as in 4.7) and B is given below:

$$B = \begin{bmatrix} -T_2 \\ -1 \\ 0 \end{bmatrix} \quad (4.27)$$

The equation of conservation of energy is

$$\left(\frac{\rho_1+\rho_2\beta_1^2}{\rho_1}\right)\frac{T}{T_2}r_1^2+\left(\frac{\rho_1+\rho_2\beta_2^2}{\rho_1}\right)\frac{T_1}{T_2}r_2^2+r_s^2=1 \quad (4.28)$$

The variation of the square root of the energy ratios with the angle of incidence and the porosity are presented in figures 4.16 and 4.17. These figures reveal that the conversion of energy into D1 and D2 waves increases with the porosity of the medium.

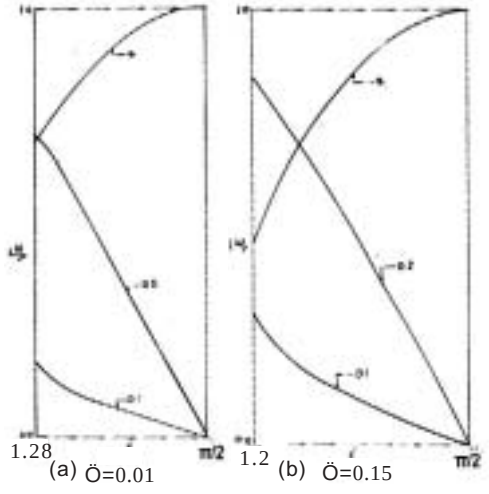

Fig.4.16 Square root of Energy ratio at rigid boundary as a function of incident angle *i* in radians for incident shear wave for porosity (a) Ö=0.10 (b) Ö=0.15.

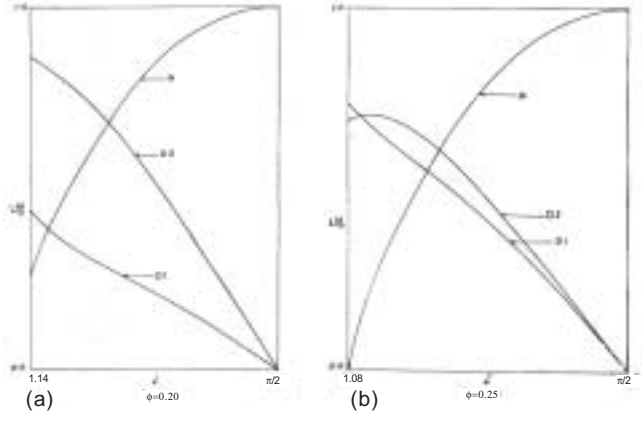

Fig.4.17 Square root of Energy ratio at rigid boundary as a function of incident angle *i* in radians for incident shear wave for porosity (a) Ö=0.20 (b) Ö=0.25. Note the increase in conversion to D1 and D2 with increase in porosity across figs 4.16 & 4.17.

5. The stress free boundary:

The expressions for the potentials for the three different cases of incident waves are the same as those given in (4.3 – 4.5), (4.19 – 4.21) & (4.24 – 4.26). With application of the boundary conditions, the matrix A in all cases turns out to be

$$A = \begin{bmatrix} k_1 & k_2 & k_3 \\ l_1 & l_2 & 0 \\ m_1 & m_2 & m_3 \end{bmatrix} \qquad (5.1)$$

The vector B is given by

$$B = \begin{bmatrix} -k_1 \\ -l_1 \\ m_1 \end{bmatrix}, \begin{bmatrix} -k_2 \\ -l_2 \\ m_2 \end{bmatrix}, \begin{bmatrix} k_3 \\ 0 \\ m_3 \end{bmatrix} \qquad (5.2)$$

for the three cases, respectively. In these expressions,

$$\begin{aligned} k_1 &= (1+T^2)(A+\beta_1 Q)+2NT^2 \\ k_2 &= (1+T_1^2)(A+\beta_2 Q)+2NT_1^2 \\ k_3 &= 2NT_2^2 \\ l_1 &= (1+T^2)(Q+\beta_1 R) \\ l_2 &= (1+T_1^2)(Q+\beta_2 R) \\ m_1 &= -2T \\ m_2 &= -2T_1 \\ m_3 &= T_2^2 - 1 \end{aligned} \qquad (5.3)$$

(The Lame's coefficient A for the solid should not be confused with the matrix A). The energy conservation equations for the three cases are

$$r_1^2 + \left(\frac{\rho_1+\rho_2\beta_2^2}{\rho_1+\rho_2\beta_1^2}\right)\frac{T_1}{T} r_2^2 + \left(\frac{\rho_1}{\rho_1+\rho_2\beta_1^2}\right)\frac{T_2}{T} r_s^2 = 1 \qquad (5.4)$$

$$\left(\frac{\rho_1+\rho_2\beta_1^2}{\rho_1+\rho_2\beta_2^2}\right)\frac{T}{T_1} r_1^2 + r_2^2 + \left(\frac{\rho_1}{\rho_2+\beta_2^2}\right)\frac{T_2}{T_1} r_s^2 = 1 \qquad (5.5)$$

$$\left(\frac{\rho_1+\rho_2\beta_1^2}{\rho_1}\right)\frac{T}{T_2} r_1^2 + \left(\frac{\rho_1+\rho_2\beta_2^2}{\rho_1}\right)\frac{T_1}{T_2} r_2^2 + r_s^2 = 1 \qquad (5.6)$$

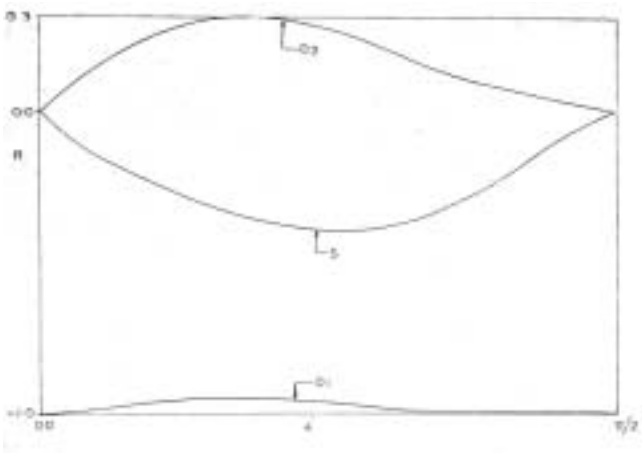

Fig.5.1 Reflectivity at stress-free boundary as a function of incident angle *i* in radians (0, ð/2) for incident D1-wave for porosity Ö=0.2

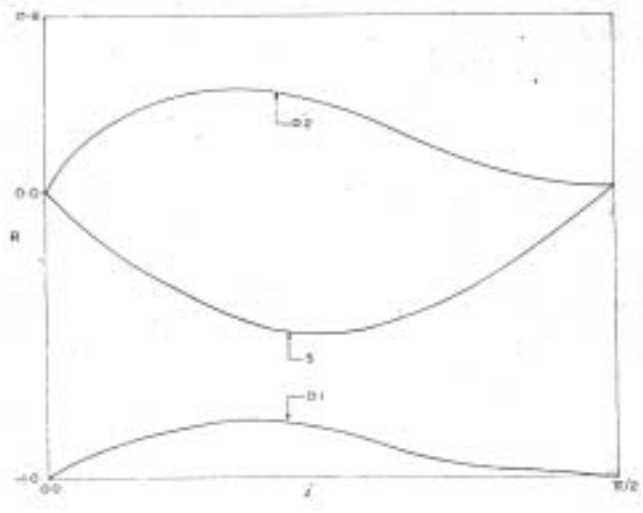

Fig.5.2 Reflectivity at stress-free boundary as a function of incident angle *i* in radians (0, ð/2) for incident D1-wave for porosity Ö=0.25

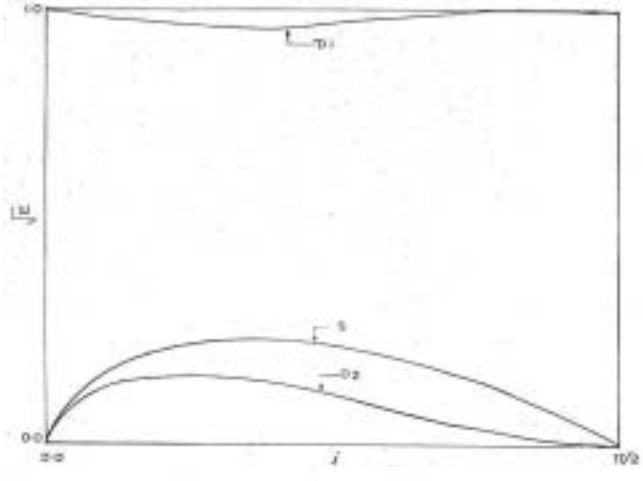

Fig.5.3 Square root of Energy ratio at stress-free boundary as a function of incident angle *i* in radians (0, ð/2) for incident D1-wave for porosity Ö=0.2

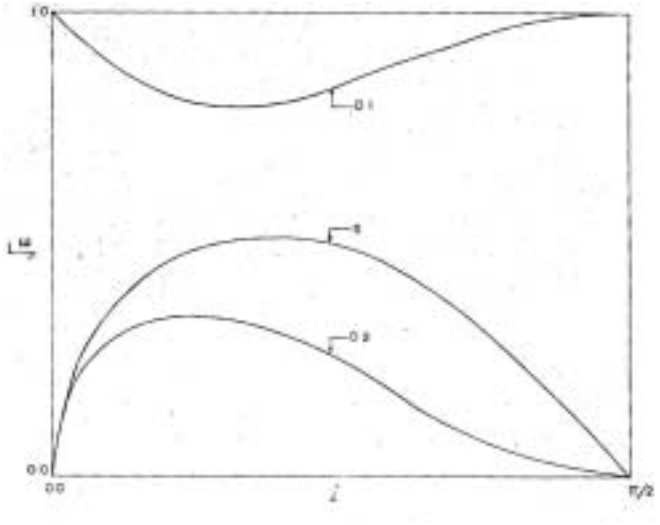

Fig.5.4 Square root of Energy ratio at stress-free boundary as a function of incident angle *i* in radians (0, ð/2) for incident D1-wave for porosity Ö=0.25

Figures (5.1) to (5.4) show the variation of the reflection coefficients and the energy with the angle of incidence, for an incident D1-wave. For small porosity, there is very little conversion of energies; r_1 is almost –1 throughout the range $(0, \pi/2)$. As the porosity increases, conversion into D2 and shear waves take place. D1 and D2 waves are always out of phase and the energy imparted to shear wave is always greater than that given to D2 wave.

The case of a D2 incident wave is described in the figures (5.5) to (5.8) .

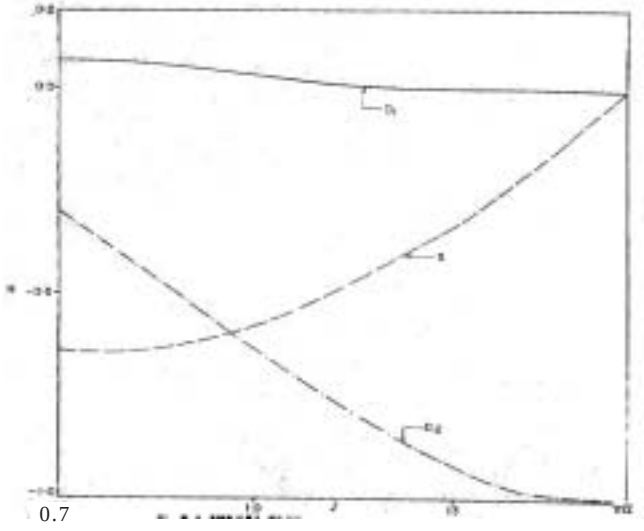

Fig.5.5 Reflectivity at stress-free boundary as a function of incident angle *i* in radians (0.7, ð/2) for incident D2-wave for porosity Ö=0.2

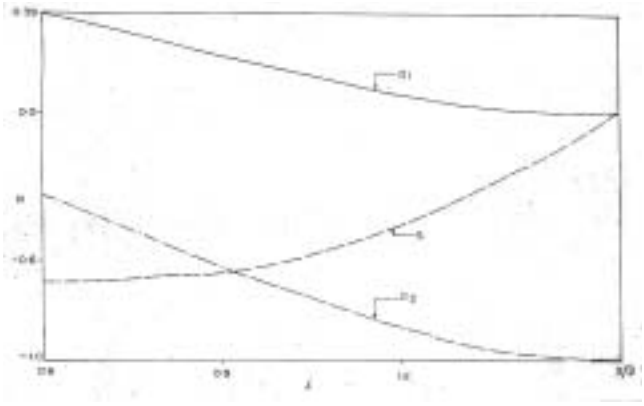

Fig.5.6 Reflectivity at stress-free boundary as a function of incident angle *i* in radians (0, ð/2) for incident D2-wave for porosity Ö=0.25

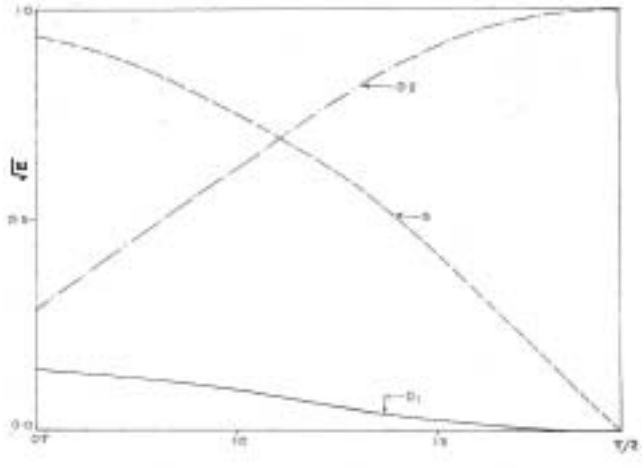

Fig.5.7 Square root of Energy ratio at stress-free boundary as a function of incident angle *i* in radians (0.7, ð/2) for incident D2-wave for porosity Ö=0.20

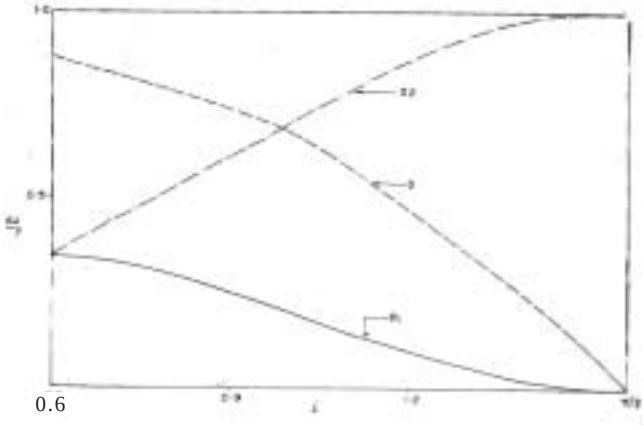

Fig.5.8 Square root of Energy ratio at stress-free boundary as a function of incident angle *i* in radians (0.6, ð/2) for incident D2-wave for porosity Ö=0.25

The case of incident Shear wave is described in the figures (5.9) to (5.10)

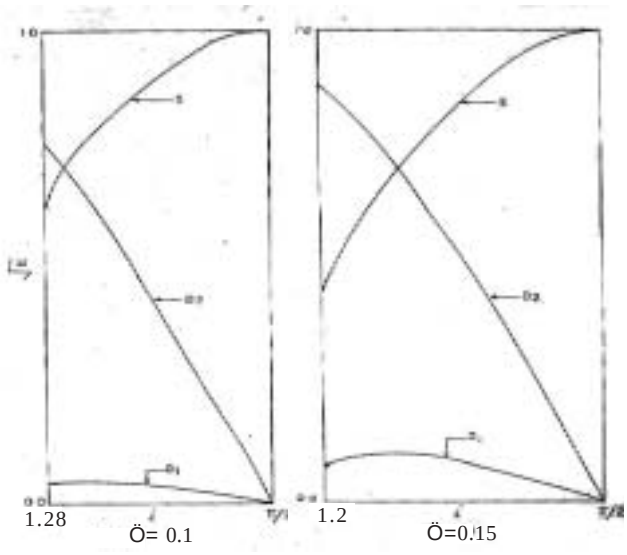

Fig.5.9 Square root of Energy ratio at stress-free boundary as a function of incident angle *i* in radians for incident Shear wave for porosity Ö=0.10 and Ö=0.15

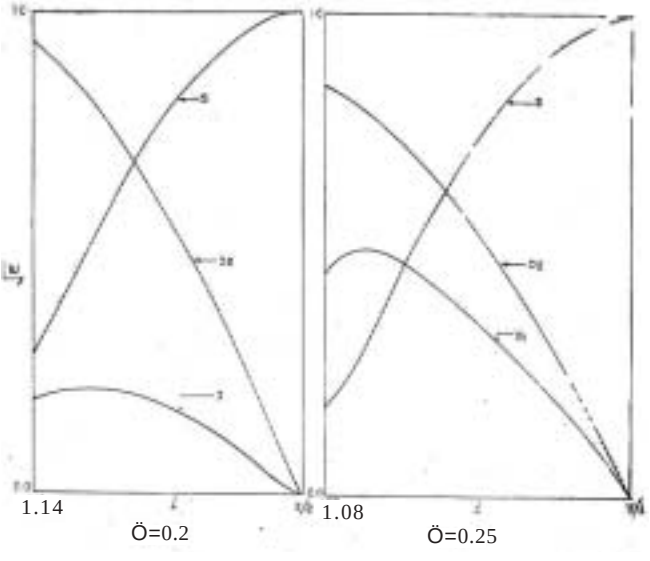

Fig.5.10 Square root of Energy ratio at stress-free boundary as a function of incident angle *i* in radians for incident Shear wave for porosity Ö=0.20 and Ö=0.25

6. The interface of two composite media:

The case of utmost interest to us is the case when any of the three kinds of wave encounters an interface of two composite media. In the following , dash denotes the transmitted medium. For an incident wave, there are three reflected waves and three transmitted waves. The expressions for the solid and the fluid potentials for the medium in which the wave is incident are the same as given earlier for different cases.

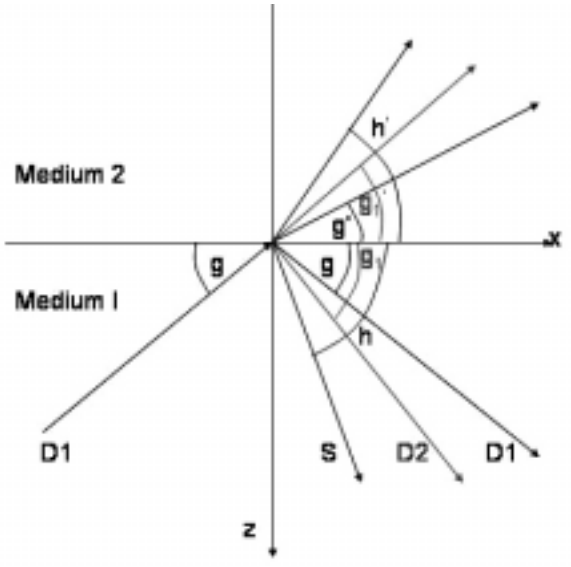

Fig.6.1 Diagram showing incident D1 and reflected/transmitted D1, D2 and S waves across interface between two porous, fluid saturated media.

In addition, the potentials for the medium in which waves are transmitted are

$$\phi_s^{'} = \phi_{sr1}^{'} \exp\left[i\left(a^{'}z - bx\right)\right] + \phi_{sr2}^{'} \exp\left[i\left(a_1^{'}z - bx\right)\right] \quad (5.7)$$

$$\phi_l^{'} = \phi_{lr1}^{'} \exp\left[i\left(a^{'}z - bx\right)\right] + \phi_{lr2}^{'} \exp\left[i\left(a_1^{'}z - bx\right)\right] \quad (5.8)$$

$$\psi_s^{'} = \psi_{sr}^{'} \exp\left[i\left(a_2^{'}z - bx\right)\right] \quad (5.9)$$

In this case also, the boundary conditions would demand that the apparent velocity along the interface (x-axis) has to be the same for all the waves and hence the coefficient b has to be same everywhere. The above expressions account for the transmitted D1, D2 and shear waves. The application of the boundary conditions yields a set of six equations for six unknowns constituting three reflection and three transmission coefficients, which are written in the matrix form:

$$AR = B \quad (5.10)$$

Where

$$A = \begin{bmatrix} k_1 & k_2 & k_3 & k_4 & k_5 & k_6 \\ l_1 & l_2 & 0 & l_3 & l_4 & 0 \\ m_1 & m_2 & m_3 & m_4 & m_5 & m_6 \\ T^{'} & T1 & 1 & T^{'} & T1^{'} & -1 \\ -1 & -1 & T2 & 1 & 1 & T2^{'} \\ \beta_1 T & \beta_2 T1 & 0 & \beta_1^{'} T^{'} & \beta_2^{'} T1^{'} & 0 \end{bmatrix} \quad (5.11)$$

$$B = \begin{bmatrix} -k_1 \\ -l_1 \\ m_1 \\ T \\ 1 \\ \beta_1 T \end{bmatrix}, \quad \begin{bmatrix} -k_2 \\ -l_2 \\ m_2 \\ T1 \\ 1 \\ \beta_2 T1 \end{bmatrix}, \quad \begin{bmatrix} k_3 \\ 0 \\ -m_3 \\ -1 \\ T2 \\ 0 \end{bmatrix} \qquad (5.12)$$

respectively, for the case of incident D1, D2 and shear waves.

$$\begin{aligned} k_1 &= (1+T^2)(A+\beta_1 Q)+2NT^2 \\ k_2 &= (1+T1^2)(A+\beta_2 Q)+2NT1^2 \\ k_3 &= 2NT2 \\ k_4 &= -\left[(1+T'^2)(A'+\beta_1' Q')+2N'T'^2\right] \\ k_5 &= -\left[(1+T1'^2)(A'+\beta_2' Q')+2N'T1'^2\right] \\ k_6 &= 2N'T2' \end{aligned} \qquad (5.13)$$

$$\begin{aligned} l_1 &= (1+T^2)(Q+\beta_1 R) \\ l_2 &= (1+T1^2)(Q+\beta_2 R) \\ l_3 &= -(1+T'^2)(Q'+\beta_1' R) \\ l_4 &= -(1+T1'^2)(Q'+\beta_2' R) \end{aligned} \qquad (5.14)$$

$$\begin{aligned} m_1 &= 2NT \\ m_2 &= 2NT1 \\ m_3 &= -N(T2^2-1) \\ m_4 &= 2N'T' \\ m_5 &= 2N'T1' \\ m_6 &= N'(T2'^2-1) \end{aligned} \qquad (5.15)$$

$$T = \tan g, \quad T1 = \tan g_1, \quad T2 = \tan h$$

$$T' = \tan g', \quad T1' = \tan g_1', \quad T2' = \tanh'$$

where g, g_1 and h, are the corresponding angles for the transmitted waves. β_1 and β_2 are expressions corresponding to β_1 and β_2 (defined earlier at 4.13 a & b) for the second medium. R is the column vector formed by the reflection and transmission coefficients:

$$R = \begin{bmatrix} r_1 \\ r_2 \\ r_s \\ t_1 \\ t_2 \\ t_s \end{bmatrix} \qquad (5.16)$$

The reflection or transmission coefficients are the ratios of the corresponding amplitudes to the incident wave amplitude.

The energy conservation equations for the three cases are:

$$r_1^2+\left(\frac{\rho_1+\rho_2\beta_2^2}{\rho_1+\rho_2\beta_1^2}\right)\frac{T1}{T}r_2^2+\left(\frac{\rho_1}{\rho_1+\rho_2\beta_1^2}\right)\frac{T2}{T}r_s^2+\left(\frac{\rho_1'+\rho_2'\beta_1'^2}{\rho_1+\rho_2\beta_1^2}\right)\frac{T'}{T}t_1^2$$
$$+\left(\frac{\rho_1'+\rho_2'\beta_2'^2}{\rho_1+\rho_2\beta_1^2}\right)\frac{T1'}{T}t_2^2+\left(\frac{\rho_1'}{\rho_1+\rho_2\beta_1^2}\right)\frac{T2'}{T}t_s^2=1 \qquad (5.18)$$

$$\left(\frac{\rho_1+\rho_2\beta_1^2}{\rho_1+\rho_2\beta_2^2}\right)\frac{T}{T1}r_1^2+r_2^2+\left(\frac{\rho_1}{\rho_1+\rho_2\beta_2^2}\right)\frac{T2}{T1}r_s^2+\left(\frac{\rho_1'+\rho_2'\beta_1'^2}{\rho_1+\rho_2\beta_2^2}\right)\frac{T1'}{T1}t_1^2$$
$$+\left(\frac{\rho_1'+\rho_2'\beta_2'^2}{\rho_1+\rho_2\beta_2^2}\right)\frac{T1'}{T1}t_2^2+\left(\frac{\rho_1'}{\rho_1+\rho_2\beta_2^2}\right)\frac{T2'}{T1}t_s^2=1 \qquad (5.19)$$

$$\left(\frac{\rho_1+\rho_2\beta_1^2}{\rho_1}\right)\frac{T}{T2}r_1^2+\left(\frac{\rho_1+\rho_2\beta_2^2}{\rho_1}\right)\frac{T1}{T2}r_2^2+r_s^2+\left(\frac{\rho_1'+\rho_2'\beta_1'^2}{\rho_1}\right)\frac{T1'}{T2}t_1^2$$
$$+\left(\frac{\rho_1'+\rho_2'\beta_2'^2}{\rho_1}\right)\frac{T1'}{T2}t_2^2+\frac{\rho_1'T2'}{\rho_1 T2}t_s^2=1 \qquad (5.20)$$

respectively.

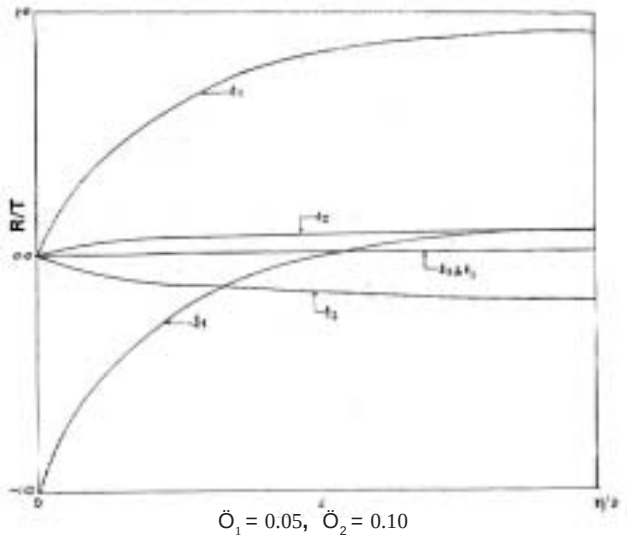

Fig.6.2 Reflection & Transmission coefficients (R/T) as a function of incidence angle ***i*** (0, ð/2) for D1, D2 and S-wave for incident D1 wave across an interface of two composite media with porosities Ö1 = 0.05 and Ö2 = 0.10

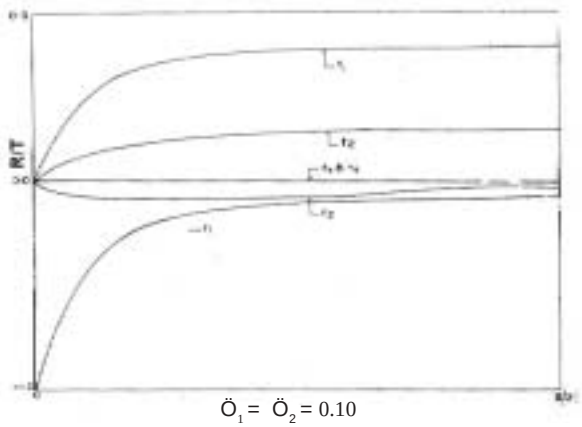

$Ö_1 = Ö_2 = 0.10$

Fig.6.3 Reflection & Transmission coefficients (R/T) as a function of incidence angle ***i*** (0, ð/2) for D1, D2 and S-wave for incident D1 wave across an interface of two composite media with porosities $Ö_1 = Ö_2 = 0.10$

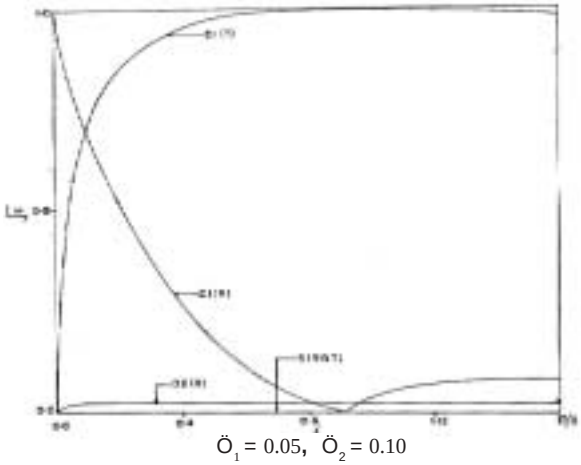

$Ö_1 = 0.05,\ Ö_2 = 0.10$

Fig.6.4 Square root of Energy ratio as a function of incidence angle ***i*** (0, ð/2) for D1, D2 and S-wave for incident D1 wave across an interface of two composite media with porosities $Ö_1 = 0.05$ and $Ö_2 = 0.10$

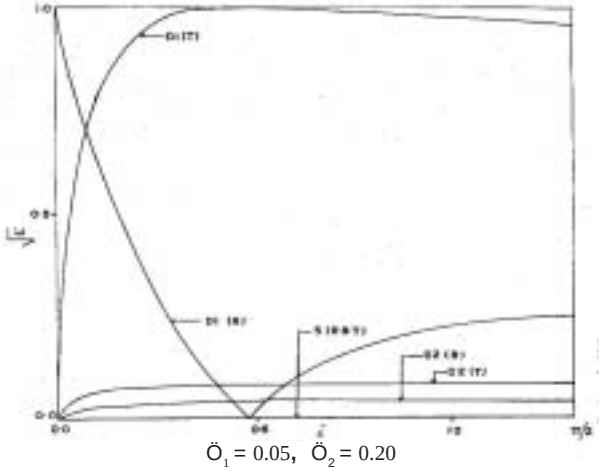

$Ö_1 = 0.05,\ Ö_2 = 0.20$

Fig.6.5 Square root of Energy ratio as a function of incidence angle ***i*** (0, ð/2) for D1, D2 and S-wave for incident D1 wave across an interface of two composite media with porosities $Ö_1 = 0.05$ and $Ö_2 = 0.20$

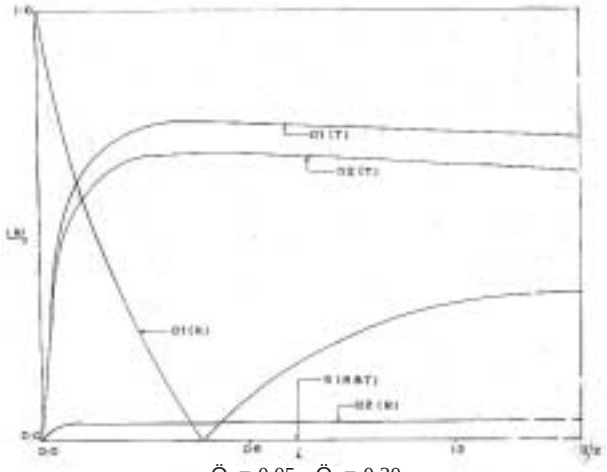

$Ö_1 = 0.05,\ Ö_2 = 0.30$

Fig.6.6 Square root of Energy ratio as a function of incidence angle ***i*** (0, ð/2) for D1, D2 and S-wave for incident D1 wave across an interface of two composite media with porosities $Ö_1 = 0.05$ and $Ö_2 = 0.30$

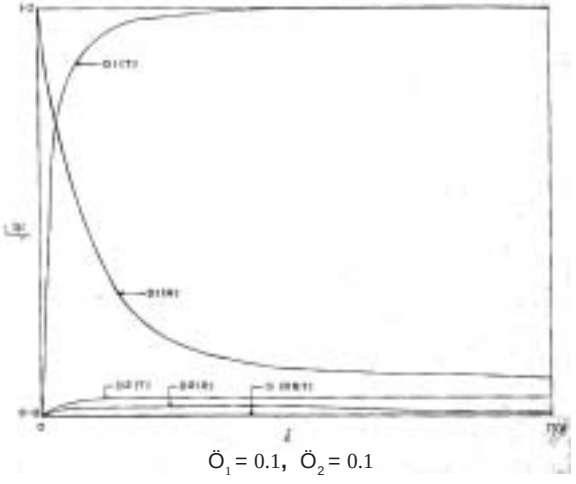

$Ö_1 = 0.1,\ Ö_2 = 0.1$

Fig.6.7 Square root of Energy ratio as a function of incidence angle ***i*** (0, ð/2) for D1, D2 and S-wave for incident D1 wave across an interface of two composite media with porosities $Ö_1 = Ö_2 = 0.10$

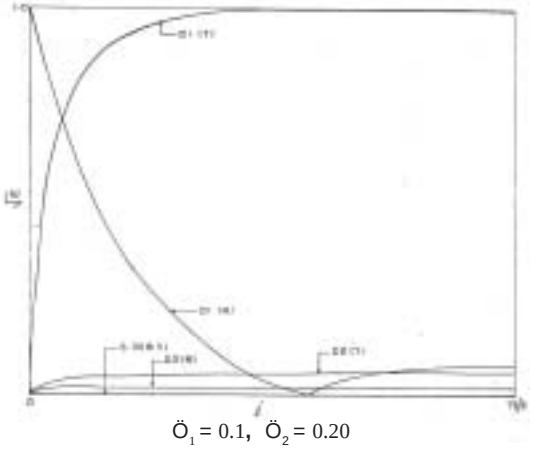

$Ö_1 = 0.1,\ Ö_2 = 0.20$

Fig.6.8 Square root of Energy ratio as a function of incidence angle ***i*** (0, ð/2) for D1, D2 and S-wave for incident D1 wave across an interface of two composite media with porosities $Ö_1 = 0.1$ and $Ö_2 = 0.20$

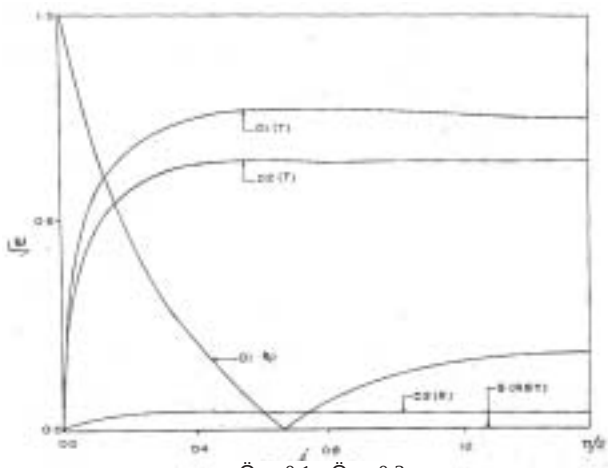

$\ddot{O}_1 = 0.1$, $\ddot{O}_2 = 0.3$

Fig.6.9 Square root of Energy ratio as a function of incidence angle ***i*** (0, ð/2) for D1, D2 and S-wave for incident D1 wave across an interface of two composite media with porosities $\ddot{O}_1 = 0.1$ and $\ddot{O}_2 = 0.30$

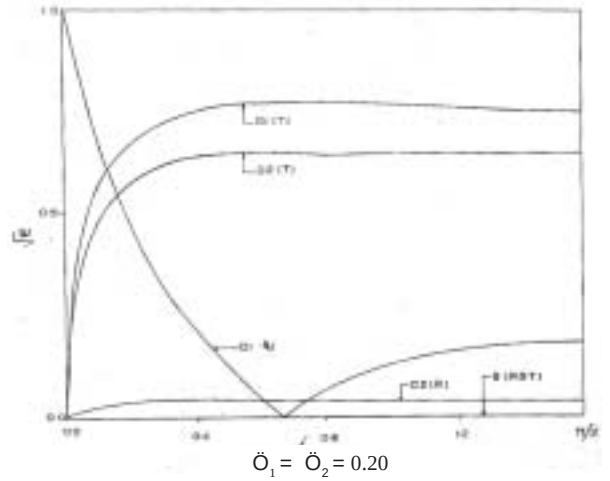

$\ddot{O}_1 = \ddot{O}_2 = 0.20$

Fig.6.10 Square root of Energy ratio as a function of incidence angle ***i*** (0, ð/2) for D1, D2 and S-wave for incident D1 wave across an interface of two composite media with porosities $\ddot{O}_1 = \ddot{O}_2 = 0.20$

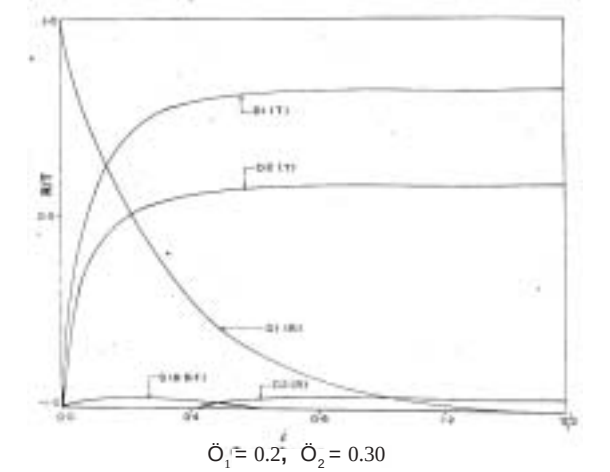

$\ddot{O}_1 = 0.2$, $\ddot{O}_2 = 0.30$

Fig.6.11 Reflection & Transmission coefficients (R/T) as a function of incidence angle ***i*** (0, ð/2) for D1, D2 and S-wave for incident D1 wave across an interface of two composite media with porosities $\ddot{O}_1 = 0.2$ and $\ddot{O}_2 = 0.30$

The figures (6.4) to (6.11) show the variation of the energy ratios with the angle of incidence and the porosities. In these figures, labels R and T in the brackets, stand for reflected and transmitted waves, respectively and s represents shear wave. For small $\ddot{O}_1$, $\ddot{O}_2$ and moderate angle of incidence significant D1- energy is transmitted as D1-energy itself. As $\ddot{O}_2$ increases, conversion of energy from D1 to D2 takes place. For $\ddot{O}_2$ as large as 0.3 an appreciable amount of energy goes into transmitted D2 wave. These figures show the existence of a critical angle where the reflected D1 energy becomes zero and transmitted D1 (and D2 & S) attains a maximum. This critical angle of incidence becomes smaller as $\ddot{O}_2$ increases. As $\ddot{O}_1$ increases, it diminishes but tends to appear again if $\ddot{O}_2$ is increased as seen in figure (6.8).

The cases of incident D2 and shear waves have also been studied and graphs have been prepared. However, we do not present them and only discuss them briefly under conclusions (Section 7).

7. Conclusions:

For the case of D1-wave incident on a rigid boundary, the effect of porosity on r_1, r_2 and r_s and the respective energies is small for near normal incidence. For a moderate angle of incidence the effect of increasing porosity is to increase the conversion into D2 and shear wave energies. For an incident D2- wave, the conversion into D1- wave energy steadily increases with the porosity, whereas the conversion into shear energy first increases and then decreases as the porosity varies from 0.05 to 0.25. When the incident wave is a shear wave, the conversion into D1 and D2 again increases with the porosity of the medium. For a stress free boundary, irrespective of the type of the incident wave, the conversion increases with increasing porosity of the medium.

For the case of a D1- wave encountering an interface of two composite media, the energies do not show any appreciable conversion as $\ddot{O}_1$ increases (keeping $\ddot{O}_2$ fixed). On the other hand as $\ddot{O}_2$ increases, mode conversion increases. Thus, the conversion and partitioning of energy essentially depends upon the porosity of the medium into which the waves are getting transmitted.

When the incident wave is a D2 or shear wave, the general tendency is to transmit out almost all energy into the second medium. For an incident D2- wave more and more energy is transferred to D1-wave as $\ddot{O}_2$ increases and the dependence on $\ddot{O}_1$ is negligible. Other energies are small. In case of incident shear wave, all energy is transmitted to the second medium as shear energy itself and the conversion into other types is very little irrespective of porosity.

Acknowledgements:

We thank all the members of the Mathematics group, in

particular Dr. C. H. Mehta, for enlightening discussions. We also thank Mr. J K Sinha of Computer Services Division for supplying a subroutine for plotting the curves. Thanks are also due to Mr. S K Choudhary and Mr. C V Subba Rao of the Exploration Division, IPE for useful discussions. Finally, good typing work of Shri B.D. Joshi is acknowledged with thanks.

References

Pan, P M. and de Bremaecker, J.C. 1970, Direct location of oil and gas by the seismic reflection method, Geoph. Pros, v13, 712.

Anstey, N.A., 1977, The New Seismic Interpreter, published by International Human Resource Development Corporation, Massachusetts, USA.

Domenico, S.N., 1974, Effect of Water saturation on seismic reflectivity of sand reservoirs on eased in shale, Geophysics, v39, 759.

Crowo and Alhilali, 1974, Amplitude of seismic events and their dependence on the absorption – dispersion pairs of the media. SEG Dallas, Also AAPG, Dallas 1975.

Biot, M.A., 1956, Theory of propagation of elastic waves in a fluid saturated porous solid I – Low frequency range. J. Acoust. Soc. Amer., 28, 168.

Biot, M.A., 1956, Theory of propagation of elastic waves in a fluid saturated porous solid II - Higher Frequency range, J. Acoust, Soc. Amer., v28, 179.

Geertsma, J. and Smit, D.C., 1961, Some aspects of elastic wave propagation in fluid saturated porous solids, Geophysics v26, 169.

Gassman, F., 1951, Elastic Waves through a packing of spheres Geophysics, v16, 673.

Ament, W.S., 1953, Sound Propagation in gross mixtures, J. Acous, Soc. Amer. v25, 638.

Wyllie, M. Gregory, A.R. and Gardner, G.H.F., 1956, Elastic wave velocities in heterogeneous and porous media, Geophysics, v21,41

Wyllie, M. Gregory, A.R. and Gardner, G.H.F., 1958, An experimental investigation of factors affecting elastic wave velocities in porous media, Geophysics, v23, 459

Wood, A.B. 1949, A text book of sound, London, G. Bell and Sons Ltd., 361.

Biot, M. A. , 1962, Mechanics of deformation and acoustic propagation in porous media, J. Appl. Phys., v33, 1482.

Biot, M.A., 1962, Generalized theory of acoustic propagation in porous dissipative media, J. Acoust, Soc. America, v34, 1254.

Toksoz, M.N., Chong C.H. and Timur A., 1976, Velocities of seismic waves in porous rocks, Geophysics, v41, 621.

Kustor, G.T. and Toksoz, M.N., 1974, Velocity and attenuation of seismic waves in two phase media, parts 1 and 2 Geophysics, v39, 587.

Stoll. R.D., 1977, Acoustic Waves in ocean sediments, Geophysics, v42, 715.

Stoll R.D., 1974, Acoustic waves in saturated sediments, physics of sound in marine sediments, Ed. L Hampton, New York.

Stoll R.D. and Bryan, G.M. 1970, Wave Attenuation in saturated sediments, J. Acoust, Soc. America, v47, 1440.

Garg, S.K., 1971, Wave propagation effects in fluid saturated porous solids J. Geophysical Res. v76, 7947.

Garg and Nur A., Effective Stress Laws for Fluid saturated porous rocks, J. Geophysics, Res., v78, 5911.

Nur, A. and Byerlee, J.D., 1971, An exact effective stress law for elastic deformation of rock with fluids, J. Geophysics, Res., v76, 6414.

Moreland, L.W., 1972,. A simple constitutive theory for a fluid saturated porous solid, J. Geophysics, Res., v77, 890.

Erwing, W.M. Jardetzky, W.S. and Press, F., 1957, Elastic Waves in Layered Media, McGraw Hill.

APPENDIX-1

The calculation of the compressional wave velocities and

If we substitute a wave form solution with wave velocity into the equations (3.2, 3.3) satisfies equation:

$$\rho_1\rho_2\alpha^4 - (P\rho_2 + R\rho_1)\,\alpha^2 + (PR - Q^2) = 0 \qquad \text{(A1.1)}$$

With the knowledge of the elastic coefficients, determined by static elastic experiments, (A1.1) gives two roots for (say α_1^2 and α_2^2) which are given by

$$\alpha_{1,2}^2 = \frac{(P\rho_2 + R\rho_1) \pm \sqrt{(P\rho_2 + R\rho_1)^2 - 4\rho_1\rho_2(PR - Q^2)}}{2\rho_1\rho_2} \qquad \text{(A1.2)}$$

α_2^2 It can be seen that α_1^2 and α_2^2 are always real and positive and α_1^2 is always greater than α_2^2. In fact it can be shown that α_1 and α_2 correspond to the D1 and D2-wave velocities in the solid and the fluid, respectively. From the equation (A1.1), if we take the limits Ö→0 and Ö →1 we get the cases of a pure solid and pure fluid medium and the equations reduce (bearing in mind that for Ö→0 or Ö→1 the coupling parameter Q vanishes) as below.

$\rho_1\alpha^2 - P = 0$ solid wave velocity

$\rho_2\alpha^2 - R = 0$ fluid wave velocity (A1.3)

(A1.2) can also be written I the form ($PR - Q^2 > 0$)

$$\alpha_{1,2}^2 = 1/2(P/\rho_1 + R/\rho_2) \pm \sqrt{\frac{1}{4}\left(\frac{P}{\rho_1} + \frac{R}{\rho_2}\right)^2 - \left(\frac{PR - Q^2}{\rho_1\rho_2}\right)} \qquad \text{(A1.4)}$$

As, $\phi \to 1$, $\rho_1 \to 0$ (with $Q \to 0$), $\alpha_1^2 \to \frac{P}{\rho_1}$ (which becomes infinite) and $\alpha_2^2 \to R/\rho_2$. Similarly, as $\phi \to 0$, $\rho_2 \to 0$ (with $Q \to 0$), $\alpha_1^2 \to \frac{P}{\rho_1}$, $\alpha_2^2 \to R/\rho_2$ (which becomes infinite). For the limiting cases, $\phi \to 0$ and $\phi \to 1$ (which correspond to the pure solid and pure fluid, respectively) the results reduce to that for solid or fluid respectively given by Erwing, Jardetzky and Press (24).

APPENDIX-2

The derivation of the boundary conditions:

When the reflector is a rigid boundary, both displacement components (solid and fluid) must vanish. These conditions in terms of the potentials and ψ_s are:

$$\begin{aligned} &\frac{\partial \phi_s}{\partial x} - \frac{\partial \psi_s}{\partial z} = 0 \\ &\frac{\partial \phi_s}{\partial z} + \frac{\partial \psi_s}{\partial x} = 0 \\ &\frac{\partial \phi_l}{\partial z} = 0 \end{aligned} \qquad \text{at z=0} \qquad \text{(A2.1)}$$

When the boundary is a stress free boundary, the normal solid and fluid stresses and the tangential solid stress must vanish:

$$\begin{aligned} &A\nabla^2\phi_s + Q\nabla^2\phi_l + 2N\left(\frac{\partial^2\phi_s}{\partial z^2} + \frac{\partial^2\psi_s}{\partial z \partial x}\right) = 0 \\ &2\frac{\partial^2\phi_s}{\partial x \partial z} + \left(\frac{\partial^2}{\partial x^2} - \frac{\partial^2}{\partial z^2}\right)\psi_s = 0 \\ &Q\nabla^2\phi_s + R\nabla^2\phi_l = 0 \end{aligned} \qquad \text{at z=0} \qquad \text{(A2.2)}$$

For the stress distribution in terms of the derivatives of the displacement components, refer to Biot (5).

For an interface of two composite media, the normal fluid and solid displacement and stress components should be continuous across the boundary. Besides, the tangential solid stress and displacements should be continuous.

Explanation of Symbols used in the figures

R	Reflection coefficients i.e., ratio of amplitudes of reflected to incident wave.
D1, D2	Dilatational waves of the 1st and 2nd kinds
S	Shear wave
i	Angle of incidence in radians.
i_{ex}	A critical angle (See pg. 11)
$Ö_1, Ö_2$	Porosities of the 1st and 2nd media. (It is understood that in the absence of a subscript there is only one porous medium)
E	Ratio of the reflected or transmitted energy to the incident energy.
r_1, r_2	Reflection coefficients of the D1, D2 waves.
t_1, t_2	Transmission coefficients of the D1, D2 waves.
r_s, t_s	Reflection and transmission coefficients of the shear wave.
D1(T)	Energy ratio for the D1 wave transmitted.
D1(R)	Energy ratio for the D1 wave reflected.
D2(T)	Energy ratio for the D2 wave transmitted
D2(R)	Energy ratio for the D2 wave reflected.
S(R)	Energy ratio for the Shear wave reflected.
ϕ_s, ψ_l S(T)	Energy ratio for the Shear wave transmitted.